Dynamic modelling of an alkaline water electrolysis system and optimization of its operating parameters for hydrogen production

Matheus H.A. Aboukalam da Cruz, Myriam Etancelin, Frédéric Marias, Jean-Michel Reneaume, Sabine Sochard-Reneaume, Sylvain Serra

Highlights
OCFE

Dynamic modelling of an alkaline water electrolysis system and optimization of its operating parameters for hydrogen production

Matheus H.A. Aboukalam da Cruz [a,*], *Myriam Etancelin* [b], *Frédéric Marias* [a], *Jean-Michel Reneaume* [a], *Sabine Sochard-Reneaume* [a], *Sylvain Serra* [a]

[a] *Universite de Pau et des Pays de l'Adour, E2S UPPA, LaTEP, Pau, France*
[b] *TERÉGA, Pau, France*

GRAPHICAL ABSTRACT

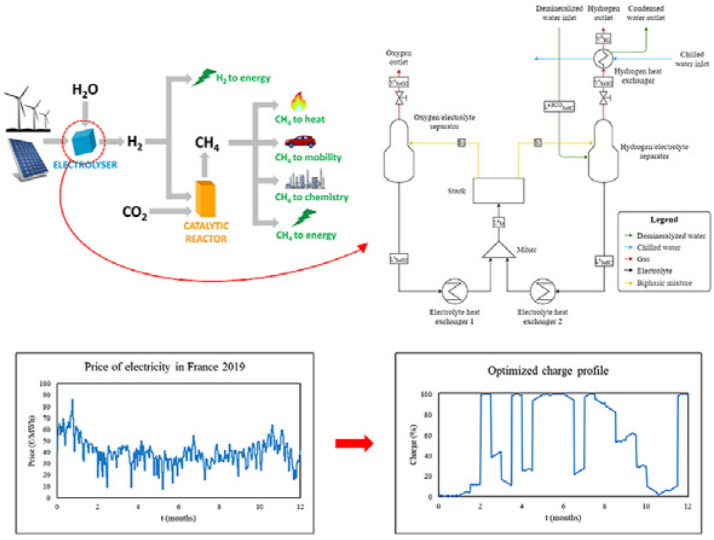

HIGHLIGHTS

- A dynamic knowledge-based model for an alkaline water electrolysis unit was created.
- OCFE was used to convert the resulting DAE set of equation into an algebraic one.
- Optimization was used to determine the evolution of the unit's operating parameters.
- The developed approach led to a 17% saving in yearly electricity cost.
- The approach seems fit to be integrated in larger dynamic optimization systems.

Keywords:
Alkaline electrolysis , Power to gas , Dynamic optimization , OCFE, Hydrogen

ABSTRACT

This work aims at developing an approach for modelling and optimizing the operation of a reference alkaline electrolysis unit operating in transient state using orthogonal colloca-tion on finite elements (OCFE). The main goal is to define the set of operating conditions that minimize the processing cost (associated to electricity cost) given a hydrogen yield. Three components of the electrolyzer are considered: the stack of electrolytic cells and two separators that single out the hydrogen and oxygen gas streams. The dynamic behavior is considered for the mass holdup in the separators as well as the energy accumulation for these three components. The associated mathematical model is derived in the paper. Its solving allows characterizing the influence of the transient operating parameters of the system on its working and associated final hydrogen production. Mathematical optimi-zation aims at defining the ideal operating load in order to minimize costs associated to fluctuating price of electricity consumed by the stack given a defined hydrogen yield. The model has been validated according to experimental test runs and operating conditions have been optimized under a proof of concept scenario saving 17% of electricity costs if compared to constant plant capacity.

Introduction

Context

Along with the growth of industrialization and global population, the consumption of fossil energies has increased significantly mainly in western countries [1]. Fig. 1 shows the evolution and projection for installed power capacity until 2025 bringing to light the major contribution of renewables such as solar and wind power. Whereas fossil fuels tend to keep their role as the main affordable supply, many companies and public organizations aim to develop new sources of energy (IEA, 2020).

The source and management of heat for industrial purposes are also great factors on the struggle against CO_2 emissions. In 2016, the generation of more than 100 EJ_{th} ($100{\cdot}10^{18}$ thermic joules) was responsible for 21% of the world's carbon dioxide emission. This heat is generated on the most part by the combustion of coal, natural gas and oil and used on processes such as the production of steam, distillation and drying [2].

In this context, many countries have determined goals related to decarbonization (decrease of fossil fuel dependency) for the next decade [3–5]. In 2015, France has implemented an act that aims to achieve renewable energy participation on 32% of energetic consumption and 40% of production before 2030. Moreover, the country seeks to decarbonize 10% of gas, which means adding to its composition a non-fossil component. The Hydrogen Deployment Plan for Energetic Transition, made by the French ministry of energetic transition, seeks to produce green hydrogen through electrolysis technology. For the hydrogen to be considered green, the electricity consumed by this process must be generated by renewable sources.

Fig. 2 describes the concept of power-to-gas. In comparison to other energy storage methods, power-to-gas can provide a long-term storage on a large scale as it can profit from the existing pipelines for natural gas. By using excess energy produced by renewable sources, it plays a great role on decarbonization [6,7]. During off-peak hours, power plants produce a low-price electricity overflow, which can be favorable for power-to-gas units to perform [8].

In order to achieve this ambitious goal, the French government, alongside with private initiative, seeks to make deep modifications on the country's energetic grid. An example of corporate action on the matter comes from TERÉGA, the transmission system operator for the French south-western gas network. In 2019, TERÉGA implemented a project called IMPULSE 2025 with the objective of conceiving a "multi-energy intelligent system" capable of interconnecting electricity, gas, heat and water grids. Because these networks are designed separately, the project aims to optimize their energetic efficiency by creating and improving intersection points (TERÉGA, 2019).

Since one of the project's goals is to investigate the production and injection of green hydrogen into the gas grid, one

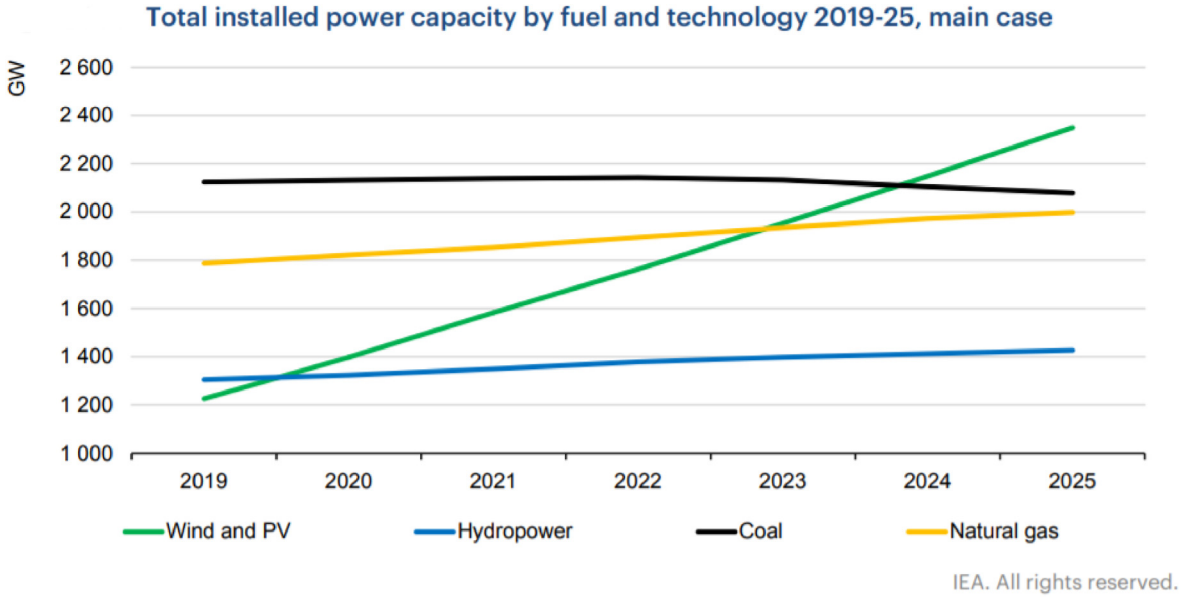

Fig. 1 – Total installed power capacity by fuel and technology between 2019 and 2025 (IEA, 2020).

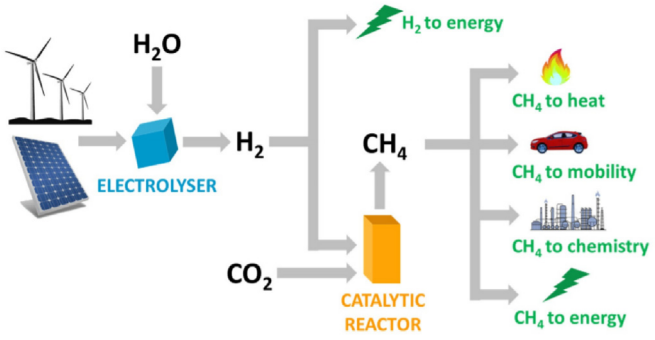

Fig. 2 – Power-to-gas routes for fuel gas production: Several fuel gases can be produced (H_2 or CH_4), according to the chosen route [7].

of these intersections connects the renewable energy grid and the gas network by means of power-to-gas. This article focuses on the development of an approach for the dynamic modelling and optimization of an alkaline water electrolysis system in the context of IMPULSE 2025. By considering the fluctuating electricity price, this work provides the optimum set of yearly operating conditions of the electrolysis system given the design of the electrolysis unit.

State of the art

This paragraph describes the scenario of scientific research on alkaline electrolysis modelling and optimization in order to give context to this work's methodologies and findings. With the surging relevance of energy transition, technologies such as water electrolysis are getting increasingly more attention from the academic community. In order to better understand it and propose innovating ideas, the modelling of this process is inevitable. Fig. 3 shows the number of publications by year on the topic, confirming it is a growing trend.

According to Olivier et al., 2017, low temperature electrolysis system models can have different objectives such as the comprehension of phenomena, performance characterization, development of control systems, durability evaluation and design. Moreover, they can be classified within four criteria:

1. The physical domain under study: electrical, thermal, chemical or fluidic [9].
2. The modelling approach: empirical or analytical.
3. The dynamic behavior: static, lumped parameters dynamic models (described by ordinary differential equations) or distributed parameters dynamic models (described by partial differential equations).
4. The modelling scale: cell/stack or auxiliaries.

In the purpose of phenomena comprehension, computational fluid dynamics (CFD) is employed to simulate dynamic distributed parameters models. They usually analyze mass and heat transfers taking place within the electrolytic cell and how they impact electrical properties and H_2 gas production [10,11]. Other models take a different approach, describing the cell as an ensemble of electric components such as resistors and diodes. This allows a better representation of the electrolyser's electric current and potential behaviors [12,13]. Since the electrolytic cell is the heart of the process, some models seek to describe its response towards change in temperature or pressure using semiempirical approaches. This means relying on physical laws but also on parameters fit to

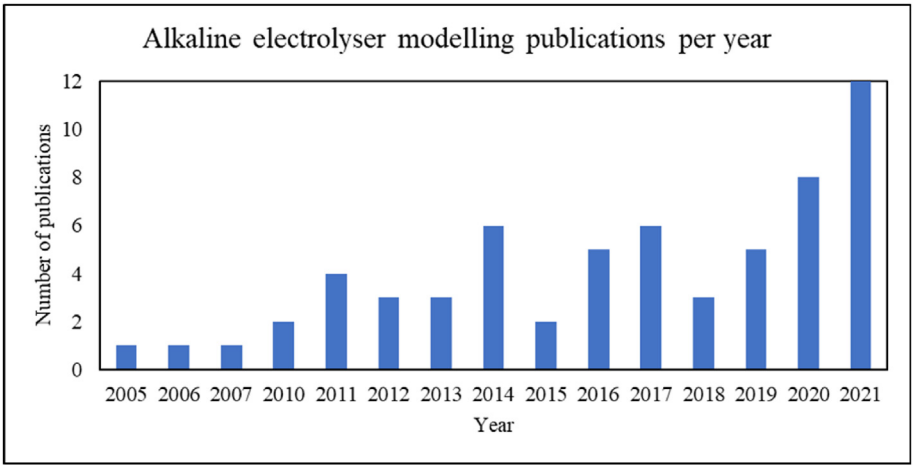

Fig. 3 – Publications by year within the alkaline electrolysis modelling subject. Source: Scopus with keywords "alkaline electrolyser (modelling OR model)".

experimental results, which can be a practical solution for optimizing the operation of electrolysis units. For example, this can be achieved by analyzing energy consumption and losses as a function of the stack's temperature [14–17] or by estimating the parameters that predict the cell's voltage as a function of electric current and temperature [18,19].

In the thermochemical domain, models are built from conservation of mass and energy, being capable to effectively include the main auxiliary processes such as the gas-liquid separators. These request more technical details concerning the unit operations in order to reach a good level of accuracy but are useful in an industrial scenario once they're capable of describing a unit's dynamic behavior [20–22]. For instance, considering the effect of bubble distribution in electrolytic cells or the diffusion of aqueous species [23,24] may increase the model's level of detail, but it may lead to higher computational effort in regard to solving. In the case where the focus is the integration of such systems with renewable energy grid, mass and energy accumulation may be neglected, relying on the energy input for describing its dynamic nature [25].

Once a model has been developed or chosen, the optimization of an electrolysis unit may take place regarding its design or its operating parameters. The optimization of its design infers varying conception parameters like electrode thickness or number of cells while operating parameters translate to the usage of already existing units [26–28].

The current work develops a model from a thermochemical perspective predicting the dynamic behavior of an alkaline electrolysis unit, making it possible to optimize its operation throughout the year considering the fluctuating electricity cost. Its equations are mostly differential and analytical since they are derived from the conservation of mass and energy as well as thermodynamic equilibria. A semiempirical approach was chosen to describe the overpotentials present in the electrolytic cells from the work of Sánchez et al., 2020. This contributes to the literature because it bridges the gap between thermal inertia and the stack's electrochemical properties, which are functions of temperature. Furthermore, dynamic optimization allows an analysis of energy consumption and cooling demand, which is particularly attractive from a process engineering perspective.

Model development

Alkaline electrolysis

As mentioned earlier, the electrolysis of water produces H_2 and O_2 gas by consuming water and energy (electricity and heat). This process takes place in a system composed of two electrodes (an anode and a cathode) submerged in an alkaline electrolytic fluid (an ion conductor). In this case, the electrolyte is usually KOH or NaOH and the ionic species responsible for electron migration are hydroxyl ions (HO^-). As the electrodes are connected to a power source, current, flows through the liquid allowing the following oxidation-reduction reactions to occur on the surfaces of each electrode.

$$\text{On the anode's: } 4\ HO^- \rightarrow 2\ H_2O + 4\ e^- + O_2 \quad (1)$$

$$\text{On the cathode's: } 4\ H_2O + 4\ e^- \rightarrow 4\ HO^- + 2\ H_2 \quad (2)$$

Therefore, the global reaction becomes [29]:

$$2\ H_2O \rightarrow 2\ H_2 + O_2 \quad (3)$$

Once it isn't a spontaneous reaction, for the production of 1 mol of hydrogen gas the system has to be fed with a specific amount of energy. It can be quantified by equation (4).

$$\Delta H^{reac} = \Delta G + T \times \Delta S \quad (4)$$

Here, ΔH indicates the total and minimal amount of supplied energy per mol, which is composed from thermal energy ($T \times \Delta S$, entropy) and electricity (ΔG, Gibbs free energy). These parameters are mostly functions of temperature. In standard conditions (25 °C and 1 bar), their values are as follows: $\Delta h^0 = 285.88$ kJ mol^{-1}, $\Delta g^0 = 237.23$ kJ mol^{-1}, and $T \times \Delta s^0 = 48.65$ kJ mol^{-1}.

Another important concept ruling the electrolytical process is the reversible voltage (U_{rev}). It is defined as the minimum voltage between electrodes for electrolysis to occur and can be related to the increase of Gibbs free energy. The latter represents the work necessary to carry out a non-spontaneous reaction at a constant temperature and pressure. Equation (5) verifies this relation.

$$U_{rev} = \frac{\Delta G}{z\,F} \quad (5)$$

Where z is the number of moles of electrons transferred for the production of 1 mol of H_2 (2 e^-) and *F* is the Faraday constant (96,500 C mol^{-1}). The value for U_{rev} in standard conditions is 1.229 V.

In fact, the cell's working voltage U_{cell} between electrodes will always be superior than the reversible voltage. This is caused by the irreversibility of the electrolysis process as well as what are called overpotentials. The three main causes for the latter:

- Activation overpotential: this is on account of the energy of activation of the partial chemical equations on each electrode. This loss is related to the limitation of load transfer speed.
- Ohmic overpotential: this is present due to the electric resistance of the electrolytic fluid and the cell's parts.
- Concentration overpotential: happens because of the resistance of mass transport through the electrolyte, which increases the concentrations of O_2 and H_2 slowing down the reaction kinetics. This loss can be disregarded at lower current densities [30].

Consequently, the estimation of the working potential of an electrolysis cell is the sum of U_{rev} and the overpotentials mentioned above. Given that these losses are mainly functions of temperature, current density and, on a minor scale, pression, empiric models are created to predict U_{cell}.

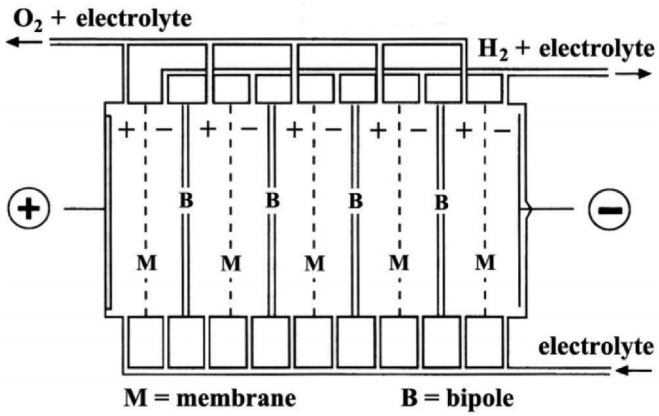

Fig. 4 – Bipolar stack scheme (adapted from Santos et al., 2013).

Equation (6) was found to be a good representative model for this scenario [31].

$$U_{cell} = U_{rev} + (r_1 + d_1 + r_2 T + d_2 p)i + s\log\left[\left(t_1 + t_2/T + t_3/T^2\right)i + 1\right] \quad (6)$$

Where r, d, s and t are overvoltage parameters related to the system, p is the cell pressure, T is the cell temperature and i is current density.

As an electrolytic cell is limited by the electrodes' surface area, increasing production requires the stacking of multiple cells. Fig. 4 shows an example of stack configuration called bipolar. *M* represents the membrane that allows ions to be exchanged but prevents gases from mixing. *B* stands for bipole, a sheet of metal that acts as cathode on the right side and anode on the left side. The cells are stacked in series from an electric perspective as the current crosses from left to right, thus making the stack's voltage the sum of those from each cell [32]. It can also be observed that the mass flow runs "in parallel" to the electric flow and that the electrolyte leaves the stack by the same outlet as the gases. Despite the endothermicity of the reaction, electric flow creates heat because of Joule effect. Thus, the electrolytic solution is pumped in excess as it plays a major role in the stack's cooling.

As seen on paragraph 2.1, for the stack to continuously produce hydrogen, it has to be cooled and the produced gas has to be separated from the liquid. Studies show that there are several thermal phenomena throughout the stack's operation that lead to a global increase of temperature [33]. For this reason, the temperature control is stablished through heat exchangers that cool the electrolyte before being fed to the stack. Hence, the cell's liquid/gas ratio has to be sufficiently high so as to ensure an effective temperature control and also prevent ohmic voltage losses [34].

System under study

Fig. 5 illustrates a simplified scheme to represent a general alkaline electrolysis unit as proposed by the literature [35,36]. To develop the methodology, a focus is held on components with fluidic or thermal inertia. As shown, there are two gas/liquid separators (one for each stack outlet). It allows the gas outlets to be monophasic and the electrolyte streams to be cooled and pumped back to the stack. In this fashion, the electrolyte (in this case potassium hydroxide) is in a closed loop while water is fed directly at the hydrogen/electrolyte separator and consumed in the stack. As mentioned on the previous paragraph, the electrolytic cells are flooded with the liquid phase. Consequently, their outlet streams are biphasic as the gas phase is composed mainly of oxygen on the anode's side and hydrogen on the cathode's. Temperature control is performed by calculating the amount of exchanged heat needed for the stack's inlet temperature to be equal to the setpoint for each electrolyte heat exchanger. If the separator's temperature is inferior to the setpoint, no heat is exchanged. Water vapor is also present on these gas phases, creating the need to dry out the stream of most interest (hydrogen, in this case). To do so, hydrogen/electrolyte separator's gas outlet goes through a heat exchanger which is also supplied with chilled glycol water. This step allows for the majority of the water vapor to condense, preparing the hydrogen stream to pass through a purification process.

Tables 1–3 list the stack's and separators' variables. For each point in time, they sum 45 variables of which 11 belong to the stack and 17 for each separator. Figs. 6–8 depict these sub-parts of the overall system in order to better understand their associated variables. The stack's diagram is simplified since its liquid and gas phases represent the sum of its cells' individual phases.

Main assumptions

The model developed in this article relies on several assumptions that allow for phenomena and mechanisms to be described on a simpler fashion so equations become less complex and computational work is spared. This is necessary for the dynamic optimization of this system as well as the optimization of bigger structures in which this system will be integrated in future works. This section is dedicated to pointing out the main assumptions and explaining why they are adopted.

Mixer

The electrolyte streams are mixed before being fed to the stack. This unit is convenient for implementing two constraints: the electrolyte's molar flow rate and KOH

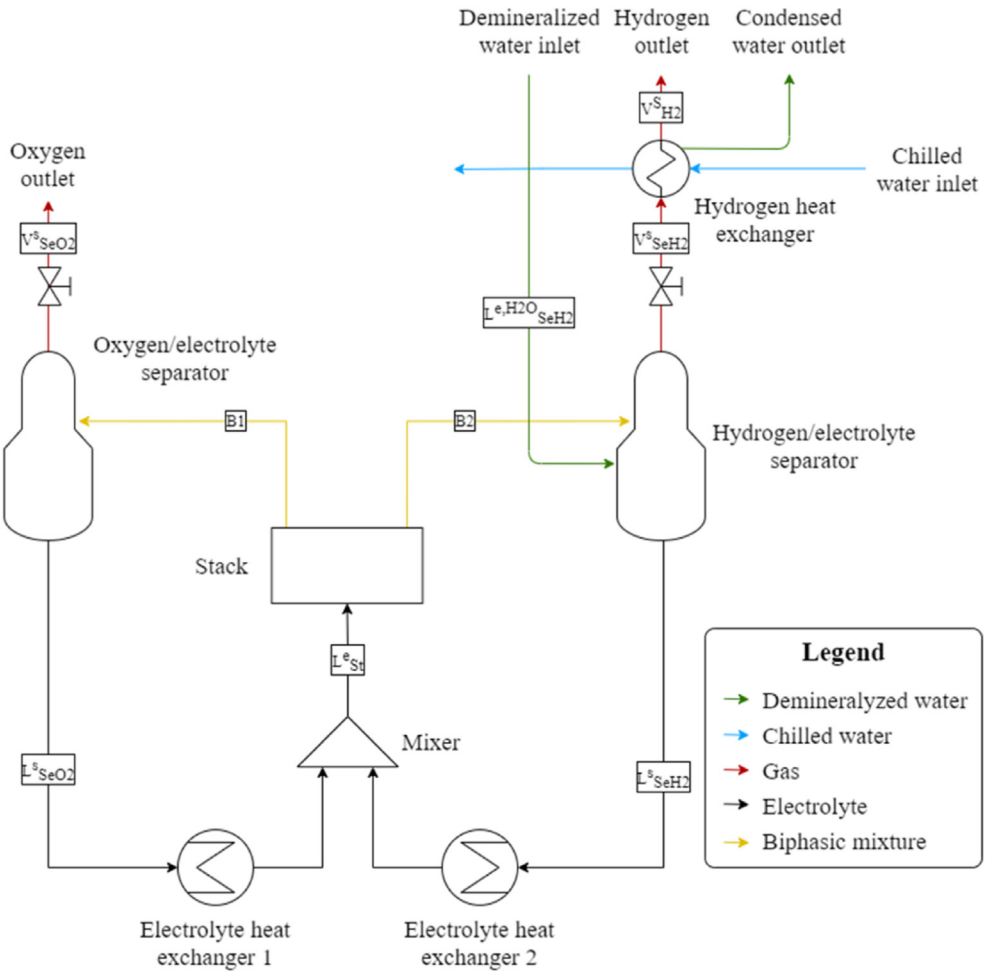

Fig. 5 – Alkaline electrolysis unit diagram.

Table 1 – Stack's problem variables.

Stack's variables

Variable	Unit	Description	Equation
x_{KOH}	–	KOH molar liquid composition	KOH molar balance (17)
x_{H2O}	–	H_2O molar liquid composition	H_2O molar balance (16)
ω^{B1}	–	Vapor fraction of biphasic outlet 1	O_2 molar balance (18)
ω^{B2}	–	Vapor fraction of biphasic outlet 2	H_2 molar balance (19)
B1	mol s^{-1}	Molar flow rate of biphasic outlet 1	Total molar balance (20)
B2	mol s^{-1}	Molar flow rate of biphasic outlet 2	Assumption Section Stack-e)
T	K	Temperature	Energy balance (21)
h^L	J mol^{-1}	Liquid specific enthalpy	h^L model (22)
H^{V1}	J mol^{-1}	Oxygen vapor phase specific enthalpy	H^{V1} model (23)
H^{V2}	J mol^{-1}	Hydrogen vapor phase specific enthalpy	H^{V2} model (24)
h^M	J kg^{-1}	Steel's specific enthalpy	h^M model (25)

Table 2 – H_2/electrolyte separator's variables.

H_2/electrolyte separator's variables			
Variable	Unit	Description	Equation
N^V	mol	Vapor phase molar holdup	Energy balance (28)
N^L	mol	Liquid phase molar holdup	Total molar balance (26)
x_{KOH}	–	KOH molar liquid composition	KOH molar balance (27)
x_{H2O}	–	H_2O molar liquid composition	H_2O molar balance (27)
x_{H2}	–	H_2 molar liquid composition	Assumption Section Thermodynamics-b)
x_{O2}	–	O_2 molar liquid composition	Assumption Section Thermodynamics-b)
y_{KOH}	–	KOH molar vapor composition	Assumption Section Thermodynamics-c)
y_{H2O}	–	H_2O molar vapor composition	Phase equilibrium (32)
y_{H2}	–	H_2 molar vapor composition	y sum (31)
y_{O2}	–	O_2 molar vapor composition	Assumption Section Thermodynamics-b)
V^{vap}	m^3	Vapor phase volume	Total volume (29)
V^{liq}	m^3	Liquid phase volume	Liquid volume (33)
T	K	Temperature	x sum (30)
h^L	J mol^{-1}	Liquid specific enthalpy	h^L model (34)
H^V	J mol^{-1}	Vapor specific enthalpy	H^V model (35)
V^s_{SeH2}	mol s^{-1}	Vapor outlet molar flow rate	Equation of state (36)
Ov	–	Valve opening	Valve equation (37)

Table 3 – O_2/electrolyte separator's variables.

O_2/electrolyte separator's variables			
Variable	Unit	Description	Equation
N^V	mol	Vapor phase molar holdup	Energy balance (40)
N^L	mol	Liquid phase molar holdup	Total molar balance (38)
x_{KOH}	–	KOH molar liquid composition	KOH molar balance (39)
x_{H2O}	–	H_2O molar liquid composition	H_2O molar balance (39)
x_{H2}	–	H_2 molar liquid composition	Assumption Section Thermodynamics-b)
x_{O2}	–	O_2 molar liquid composition	Assumption Section Thermodynamics-b)
y_{KOH}	–	KOH molar vapor composition	Assumption Section Thermodynamics-c)
y_{H2O}	–	H_2O molar vapor composition	Phase equilibrium (44)
y_{H2}	–	H_2 molar vapor composition	Assumption Section Thermodynamics-b)
y_{O2}	–	O_2 molar vapor composition	y sum (43)
V^{vap}	m^3	Vapor phase volume	Total volume (41)
V^{liq}	m^3	Liquid phase volume	Liquid volume (45)
T	K	Temperature	x sum (42)
h^L	J mol^{-1}	Liquid specific enthalpy	h^L model (46)
H^V	J mol^{-1}	Vapor specific enthalpy	H^V model (47)
V^s_{SeO2}	mol s^{-1}	Vapor outlet molar flow rate	Equation of state (48)
Ov	–	Valve opening	Valve equation (49)

concentration. Specifying these features is necessary for mathematical convergence as hydroxide potassium is in a closed loop.

Thermodynamics

These assumptions seek to simplify enthalpy calculations as well as fluid phase equilibria.

a) Ideal and uniform phases

Intermolecular interactions are neglected and both gas and liquid phases are considered to have uniform properties in order to simplify the equilibrium calculations.

b) H_2 and O_2 solubilities on liquid phase are neglected

Hydrogen and oxygen molecules are considered to exist only in gaseous phase due to their low solubility in potassium hydroxide solution. This assumption is supported once the molar fraction in liquid water for both gases are around $3{\cdot}10^{-4}$ at temperature and pressure similar of the stack (NIST database). For KOH solutions, the absorption of these gases tend to be even smaller [37,38]. The main consequence of this assumption is that hydrogen and oxygen mixing is impossible, once the liquid phase won't serve as a bridge between the two gas phases through absorption/desorption.

$$x_{H_2} = x_{O_2} = 0 \tag{7}$$

c) KOH volatility is neglected

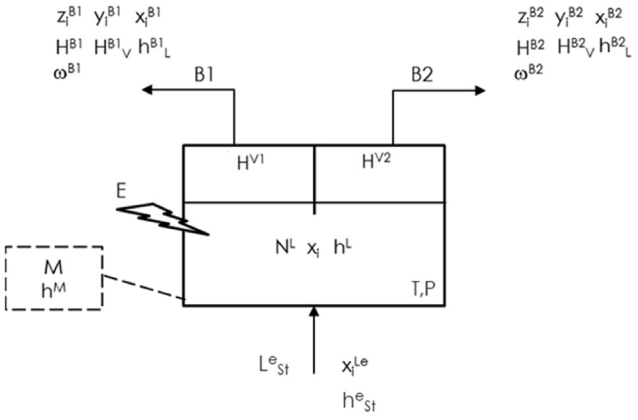

Fig. 6 – Stack's simplified diagram.

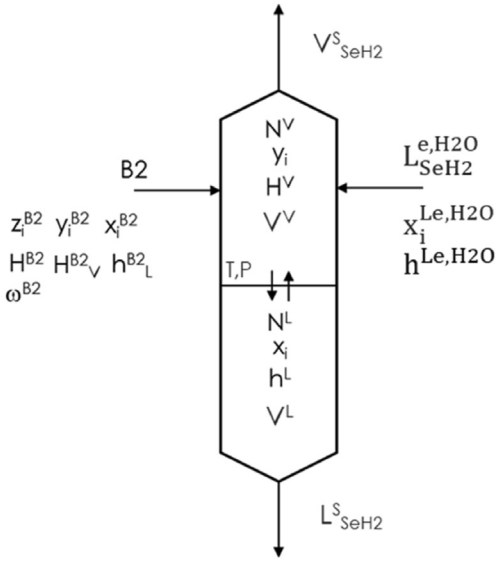

Fig. 7 – H_2/electrolyte separator's simplified diagram.

The phase equilibrium of potassium hydroxide was disregarded as its volatility is negligible at process conditions. This can be verified as the KOH solution at real concentration, pressure and temperature would produce a gas phase with a molar fraction of around $1.15 \cdot 10^{-3}$ [39]. Thus, the electrolyte cannot exit the system by the gas streams, being enclosed in the loop (stack and separators).

$$y_{KOH} = 0 \tag{8}$$

d) All of the heat capacities are considered constants regarding temperature
e) Electrolyte's heat capacity is a function of its composition

The solution's heat capacity (Cp^L_{elec}) was considered to be a function of its composition. For this reason, equation (9) was

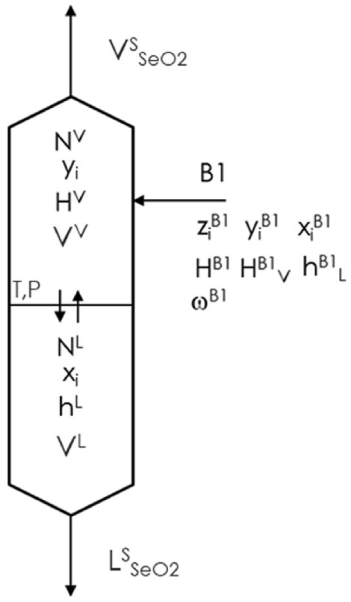

Fig. 8 – O_2/separator's simplified diagram.

stablished as a polynomial correlation of the potassium hydroxide's molar fraction (x_{KOH}). It was originated from the interpolation of data found in literature and returns the heat capacity in J mol^{-1} K^{-1} [40].

$$Cp^L_{elec} = 4936.909\, x^4_{KOH} - 3843.66\, x^3_{KOH} + 997.947\, x^2_{KOH} - 126.364\, x_{KOH} + 75.09 \tag{9}$$

f) Water's latent heat of vaporization is constant

Since water is the only phase-changing species in the system, its enthalpy of vaporization was chosen to be constant.

g) Unit operations are adiabatic

In the sake of simplicity, all heat losses from unit operations to the surroundings are neglected.

Control

There are three main variables controlled by supervision systems on the unit: the electrolyte temperature; the hydrogen's final outlet temperature and the separators' internal pressures. The following strategies were adopted to simulate these control loops.

a) Heat exchangers

In the unit's electrolyte cooling system, the glycol water's flow rate is controlled to respect a maximum temperature setpoint. For this reason, the exchanged heat is zero until the electrolyte's temperature reaches this setpoint. If the temperature tends to exceed its maximum value, it is fixed at the setpoint and the exchanged heat (now greater than zero)

becomes a new variable. The glycol water's flow rate or temperatures are not taken into consideration.

However, for the hydrogen cooling heat exchanger the glycol water's properties are considered as its mass flow rate is a problem's variable. It is calculated to provide enough exchanged heat for the hydrogen gas to exit at a fixed temperature. Moreover, a water phase equilibrium is present in this equipment to simulate water condensation. That defines the gas outlet's water content and the liquid water outlet's mass flow rate. The equilibrium, like in the separators, is also calculated from ideal phases (equation (15)).

b) Gas outlet valves

The valves shown in Fig. 5 above the separators were modelled with the objective of regulating the vessels' pressures. Each of them is described by their own equation on the format of equation (10) below.

$$\dot{V}_{gas} = Kv \cdot Ov \sqrt{\Delta P} \tag{10}$$

Where $\dot{V}_{gas}$ represents the gas stream's volumetric flow rate ($m^3\,s^{-1}$), Kv the valve's constant ($m^3\,s^{-1}\,Pa^{-1/2}$), Ov the opening varying from 0 (closed) to 1 (open) and ΔP the pressure difference between the two sides of the valve (Pa). This equation allows for ΔP to be fixed at a setpoint while Ov is the variable responsible for the regulation.

Stack

In virtue of the stacks great complexity and need for specific details, the following assumptions were adopted.

a) Vapor phases' energy holdup is neglected

In the view of the liquid phase's predominant contribution to thermal inertia, vapor phases' energy holdup is neglected for the sake of model simplicity.

$$\frac{d(N^{V1}H^{V1})}{dt} = \frac{d(N^{V2}H^{V2})}{dt} = 0 \tag{11}$$

b) Matter holdup is neglected

The great majority of the cells' volumes are filled with the electrolyte solution at all times, which is assumed to be incompressible. This fact results in a practically constant amount of matter (holdup) during operation, allowing to disregard its derivative with respect to time (equation (12)). However, it is important to point out that this assumption is not applied to the accumulation of energy as the stack can present "thermal inertia".

$$\frac{dN^{V1}}{dt} = \frac{dN^{V2}}{dt} = \frac{dN^{L}}{dt} = 0 \tag{12}$$

c) Liquid-vapor equilibrium is neglected

Since the stack's biphasic outlets are fed to the separators, these are the main source of water in gas phase due to their phase equilibria. Therefore, considering a gas-liquid equilibrium in the stack wouldn't add to the gas phases' water content, only increase computation time. For this reason, hydrogen and oxygen leaving the stack are free of water vapor.

$$y_{H_2O} = 0 \tag{13}$$

d) Single liquid phase

Due to the electrolyte's global excess with respect to the consumption of water, the change on its composition is minimal. For this reason, it was considered that the liquid phase isn't separated by electrode type like in Fig. 4. Instead, both anode and cathode sides share the same electrolyte composition and temperature.

e) Uniform electrolyte distribution at outlets

The stack's biphasic outlets are considered to have the same resistance to liquid flow. That translates to the same molar flow rate of liquid for both outlets, as expressed on equation (14) below. It assures that despite variation on vapor fraction (ω) and total molar flow rate (*B1* and *B2*), the same amount of liquid is transmitted to the separators.

$$B1 \cdot (1 - \omega^{B1}) = B2 \cdot (1 - \omega^{B2}) \tag{14}$$

f) Electrolytic cell's voltage is a function of temperature, pressure and current

In order to describe the stack's operating voltage, equation (6) was adopted.

Gas-liquid separators

The following assumptions support the interpretation of the gas-electrolyte separators as flash vessels. That means its outlet streams are in thermodynamic equilibrium which ties their pressure, temperature and water content.

a) Liquid-vapor equilibrium of water is stablished

It is considered that the liquid and the gas phases in the separators are in equilibrium. In light of assumptions Section Thermodynamics-b) and c), water is the only species transferred from the liquid to the gas phase. Since assumption Section Thermodynamics-a) implies that activity and fugacity coefficients are equal to 1, Raoult's law represents this equilibrium through equation (15).

$$x_{H_2O}\, P^{sat}_{H_2O} = y_{H_2O}\, P \tag{15}$$

Where *x* and *y* stand respectively for water's molar fraction on the liquid and gas phase, P^{sat} for saturation pressure and *P* for pressure (both in Pa).

System of equations

In order to simulate the system's operation, the number of problem variables needs to equal the number of independent equations describing it. In this configuration, for a given initial state and constant parameters, there is a unique solution that satisfies the system of equations describing the device's behavior through time. Disturbances like parameter variation leads to a different solution.

Table 4 describe the stack's contribution to the problem's equations. There are 10 equations that when combined to assumption Section Stack-e) cancel out the degrees of freedom for its simulation. Tables 5 and 6 describe the H_2/electrolyte and O_2/electrolyte separators' contribution to the problem's equations. There are 13 equations each that when combined to assumptions Section Thermodynamics-b) and c) cancel out the degrees of freedom for its simulation. The liquid volumes, see equations (33) and (45), are functions of the KOH solution's density. To determine it, an empirical correlation was proposed based on experimental data [41].

Mathematical relations

In addition to the main set of equations described above on paragraph 2.4, the model needs complementary relations that are functions of the problem's variables and help simplifying the final form of the equations. Tables 7 and 8 describe these relations for the stack and the separators, respectively.

The extent of global reaction (equation (50)) is directly proportional to the electric current passing through the stack. The constant K_ξ's value is equal to $2\,F = 192970.66$ A s mol^{-1} and was obtained theoretically from the statement: for each 2 mol of electrons passing through a cell, 1 mol of H_2 is produced. Equations (52) and (53) for the enthalpy of reaction and reversible potential were stablished from thermodynamic data found in the literature by adapting high temperature data to the system's low temperature [42]. The cell's voltage is given by equation (6).

Solving

The final set of equations, as it is shown on Tables 1–6 is categorized as differential-algebraic and nonlinear. To solve it, the orthogonal collocation method on finite elements (OCFE) will firstly convert it into a completely algebraic system. An explanation on the method's approach is available in the Appendix section.

At $t = 0$, the unit is considered to be at steady state. This means that the derivatives of all variables with respect to time equal zero. Thus, at the following time step, where a disturbance occurs, the steady state variables are the initialization point for the solving of the transient state model. The separators' given initial state is defined by their pressure and liquid level (60% in this case).

The chosen Integrated Development Environment to simulate and optimize (see paragraph 4.2) the alkaline electrolytic unit is AMPL. Once the user has stated all of the problem's parameters, variables, objective function and constraints, it will use the selected solver to find a solution that satisfies all of the equations. In this case, the chosen solver and code editor were, respectively, CONOPT and Visual Studio Code.

Although it is originally conceived to solve optimization problems, AMPL can also solve non-linear systems of equation in order to simulate the unit's operation. The difference is that in optimization the number of variables is greater than the number of constraints, whereas in simulation their number are equal, transforming it into a feasibility problem.

Fig. 9 represents the code's flowchart for simulation. It was found that solving each finite element at a time helps reducing the global simulation time. This is attributed to the fact that the element's variables initial values are equal to the previous element's last value, which is closer to the solution. In contrast, this choice can't be made in optimization problems as all elements must be optimized at the same time, meaning the loop in Fig. 9 gives place to the solving of a unique larger system of equations.

Table 4 – Stack's problem equations.

Stack's equations

Name	Equation	N°
H_2O molar balance [mol s^{-1}]	$0 = L^e_{St} x^e_{H2O} - x_{H2O}(1-\omega^{B1})B1 - x_{H2O}(1-\omega^{B2})B2 + \nu_{H2O}\xi$	(16)
KOH molar balance [mol s^{-1}]	$0 = L^e_{St} x^e_{KOH} - x_{KOH}(1-\omega^{B1})B1 - x_{KOH}(1-\omega^{B2})B2$	(17)
O_2 molar balance [mol s^{-1}]	$0 = -\omega^{B1}B1 + \nu_{O2}\,\xi$	(18)
H_2 molar balance [mol s^{-1}]	$0 = -\omega^{B2}B2 + \nu_{H2}\,\xi$	(19)
Total molar balance [mol s^{-1}]	$0 = L^e_{St} - B1 - B2 + \sum_i \nu_i \xi$	(20)
Energy balance [J s^{-1}]	$\frac{d(N^L h^L)}{dt} + \frac{d(M\,h^M)}{dt} = E + L^e_{St}\,h^e_{St} - B1\,H^{B1} - B2\,H^{B2} - \Delta H^{reac}\,\xi$	(21)
h^L model [J mol^{-1}]	$h^L = Cp^L_{elec}\,(T - T_{ref})$	(22)
H^{V1} model [J mol^{-1}]	$H^{V1} = Cp^V_{H2}\,(T - T_{ref})$	(23)
H^{V2} model [J mol^{-1}]	$H^{V2} = Cp^V_{O2}\,(T - T_{ref})$	(24)
h^M model [J kg^{-1}]	$h^M = Cp^S_{steel}\,(T - T_{ref})$	(25)

Table 5 – H_2/electrolyte separator's equations.

H_2/electrolyte separator's equations

Name	Equation	N°
Total molar balance [mol s^{-1}]	$\frac{dN^V}{dt}+\frac{dN^L}{dt}=L^{e,H2O}_{SeH2}+B2-L^{s}_{SeH2}-V^{s}_{SeH2}$	(26)
Partial molar balance [mol s^{-1}]	$\frac{d(N^V y_i)}{dt}+\frac{d(N^L x_i)}{dt}=L^{e,H2O}_{SeH2}\,x_i^{Le,H2O}+B2\,z_i^{B2}-L^{s}_{SeH2}\,x_i-V^{s}_{SeH2}\,y_i$	(27)
Energy balance [J s^{-1}]	$\frac{d(N^V H^V-P^V V^V)}{dt}+\frac{d(N^L h^L-P^L V^L)}{dt}=L^{e,H2O}_{SeH2}\,h^{Le,H2O}+B2\,H^{B2}-L^{s}_{SeH2}\,h^L-V^{s}_{SeH2}\,H^V$	(28)
Total volume [m^3]	$V^{tot}=V^{liq}+V^{vap}$	(29)
x sum	$\sum_i x_i=1$	(30)
y sum	$\sum_i y_i=1$	(31)
Phase equilibrium	$y_{H2O}=\frac{P^{sat}_{H2O}}{P}x_{H2O}$	(32)
Liquid volume [m^3]	$V^{liq}=N^L(-8.49\,x^3_{KOH}+6.24\,x^2_{KOH}-1.02\,x_{KOH}+1.84)\cdot10^{-5}$	(33)
h^L model [J mol^{-1}]	$h^L=Cp^L_{élec}\,(T-T_{ref})$	(34)
H^V model [J mol^{-1}]	$H^V=\sum_i y_i\,H^V_i$	(35)
	$H^V_{H2}=Cp^V_{H2}\,(T-T_{ref})$	
	$H^V_{H2O}=Cp^L_{H2O}\,(T_{eb}-T_{ref})+\Delta H^{vap}+Cp^V_{H2O}\,(T-T_{ref})$	
Equation of state [Pa m^3]	$P\,V^{vap}=N^V\,R\,T$	(36)
Valve equation [m^3 s^{-1}]	$\frac{V^{s}_{SeH2}\,R\,T}{P}=Kv\,Ov\,\sqrt{\Delta P}$	(37)

Table 6 – O_2/electrolyte separator's equations.

O_2/electrolyte separator's equations

Name	Equation	N°
Total molar balance [mol s^{-1}]	$\frac{dN^V}{dt}+\frac{dN^L}{dt}=B1-L^{s}_{SeO2}-V^{s}_{SeO2}$	(38)
Partial molar balance [mol s^{-1}]	$\frac{d(N^V y_i)}{dt}+\frac{d(N^L x_i)}{dt}=B1\,z_i^{B1}-L^{s}_{SeO2}\,x_i-V^{s}_{SeO2}\,y_i$	(39)
Energy balance [J s^{-1}]	$\frac{d(N^V H^V-P^V V^V)}{dt}+\frac{d(N^L h^L-P^L V^L)}{dt}=B1\,H^{B1}-L^{s}_{SeO2}\,h^L-V^{s}_{SeO2}\,H^V$	(40)
Total volume [m^3]	$V^{tot}=V^{liq}+V^{vap}$	(41)
x sum	$\sum_i x_i=1$	(42)
y sum	$\sum_i y_i=1$	(43)
Phase equilibrium	$y_{H2O}=\frac{P^{sat}_{H2O}}{P}x_{H2O}$	(44)
Liquid volume [m^3]	$V^{liq}=N^L(-8.49\,x^3_{KOH}+6.24\,x^2_{KOH}-1.02\,x_{KOH}+1.84)\bullet10^{-5}$	(45)
h^L model [J mol^{-1}]	$h^L=Cp^L_{élec}\,(T-T_{ref})$	(46)
H^V model [J mol^{-1}]	$H^V=\sum_i y_i\,H^V_i$	(47)
	$H^V_{O2}=Cp^V_{O2}\,(T-T_{ref})$	
	$H^V_{H2O}=Cp^L_{H2O}\,(T_{eb}-T_{ref})+\Delta H^{vap}+Cp^V_{H2O}\,(T-T_{ref})$	
Equation of state [Pa m^3]	$P\,V^{vap}=N^V\,R\,T$	(48)
Valve equation [m^3 s^{-1}]	$\frac{V^{s}_{SeO2}\,R\,T}{P}=Kv\,Ov\,\sqrt{\Delta P}$	(49)

Results

As mentioned in paragraph 3, optimization problems contain more variables than constraints. For this reason, it exists an infinite number of solutions capable of satisfying the problem's equations where the exceeding variables may assume different values. The goal is to find a solution among those that also maximizes the objective function, which is the mathematical representation of the criteria that favors some solutions over others. Prior to optimization, a simulation step is required to validate the model.

Simulation and validation

To check the model behavior, a simulation run illustrating load changes of the electrolysis unit is carried out. It begins at full stop, raising to 80% of its capacity, followed by 100% and

Table 7 – Stack's complementary equations.

Name	Equation	N°
Extent of global reaction [mol s^{-1}]	$\xi = n_{cells}\ \frac{I}{K_\xi}$	(50)
Electrical power consumed [W]	$E = n_{cells}\ U_{cell}\ I$	(51)
Enthalpy of reaction [J mol^{-1}]	$\Delta H^{reac} = -33.069484\ T + 2.9574 \cdot 10^5$	(52)
Reversible voltage [V]	$U_{rev} = -8.02156 \cdot 10^{-4}\ T + 1.46726$	(53)
Cell's voltage [V]	$U_{cell} = U_{rev} + (r_1 + d_1 + r_2 T + d_2\ p)i + s\ \log\left[\left(t_1 + t_2/T + t_3/T^2\right)i + 1\right]$	(6)
Molar enthalpy of B1 stream [J mol^{-1}]	$H^{B1} = H^{V1}\ \omega^{B1} + h^L(1 - \omega^{B1})$	(54)
Molar enthalpy of B2 stream [J mol^{-1}]	$H^{B2} = H^{V2}\ \omega^{B2} + h^L(1 - \omega^{B2})$	(55)
Molar fraction of B1 stream	$z_i^{B1} = y_i^{B1}\ \omega^{B1} + x_i^{B1}(1 - \omega^{B1})$	(56)
Molar fraction of B2 stream	$z_i^{B2} = y_i^{B2}\ \omega^{B2} + x_i^{B2}(1 - \omega^{B2})$	(57)
Liquid molar holdup [mol]	$N^L = \frac{1000\ m^L}{\sum_{i=H2O,KOH} Mmol_i\ x_i}$	(58)

Table 8 – Separators' complementary equations.

Name	Equation	N°
Water's saturation pressure [Pa]	$P_{H2O}^{sat} = \exp(A + \frac{B}{T} + C \log T + D\ T^E)$	(59)
Liquid molar enthalpy of demineralized water [J mol^{-1}]	$h^{LeH2O} = Cp_{H2O}^L\ (T^{Le} - T_{ref})$	(60)

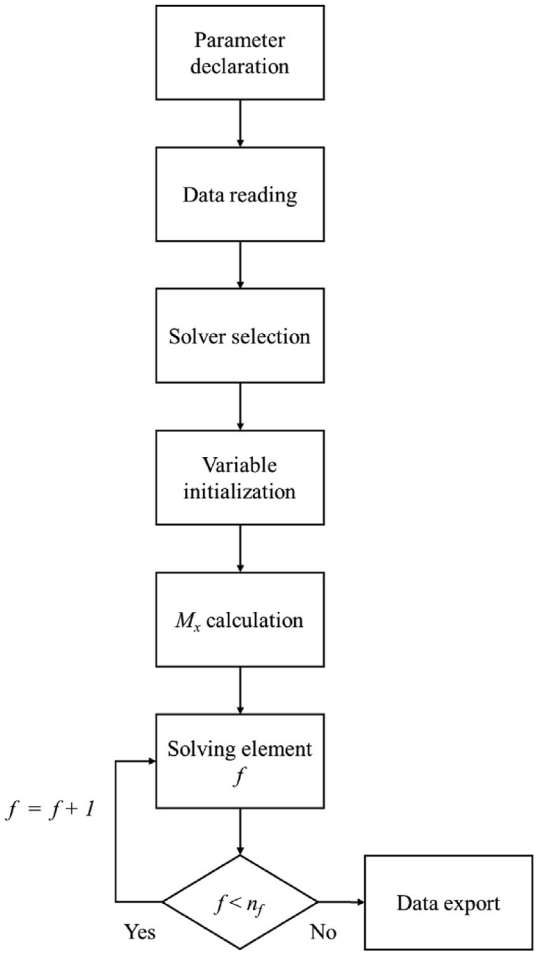

Fig. 9 – AMPL code's flowchart for simulation.

then returning to 0%. Results concerning the electrolytic stack are compared to experimental ones and are reported in Figs. 10–12 in variables are normalized (all values are divided by the biggest value obtained). Dots represent data that behave as expected given the chosen approach and assumptions. The root mean square error for the voltage, temperature and H_2 volumetric flow rate represented by dots is 0.045, 0.118 and 0.047. It can be observed that voltage is proportional to temperature and that the latter's variation considers the system's mass and energy inertia. Also, rapid changes in H_2 volumetric flowrate are observed, which agrees with experimental data. This happens because H_2 flowrate should be a function mainly of electric current while temperature and voltage are the variables most affected by the system's thermal inertia.

Triangles represent data that is imprecise due to the low reproducibility of the test run such as the lack of information concerning the behavior of heat exchangers and pumps during load change. These are attributed to the parameter estimation of the stack's voltage correlation (equation (6)), which could be improved with calibration considering more real equipment data. Moreover, when the electrolyzer isn't operating (as observed between instants 0.8 and 1), the predicted voltage is not zero. However, this does not reflect on temperature neither on hydrogen production as these are mainly function of electric current, which is zero at full stop. This allows to confirm that the approach developed here is relevant to study the dynamic behavior of this unit.

Figs. 13 and 14 represent the evolution of normalized liquid KOH and vapor H_2O molar fractions for H_2/electrolyte and O_2/electrolyte separators respectively. Electrolyte's concentration varies negligibly due to the fact that it is a closed system for potassium hydroxide and that mass accumulation is dampened by the imposed liquid molar flows leaving the separators proportional to the unit's current load. The variation of water molar fraction in the gas phases are mainly a function of

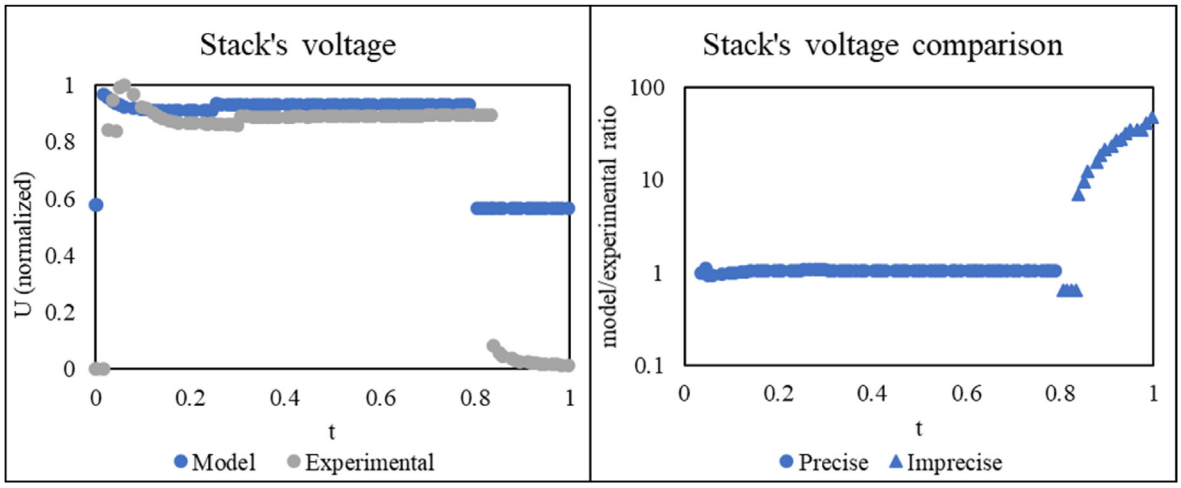

Fig. 10 – Normalized stack's voltage and model/experimental results ratio.

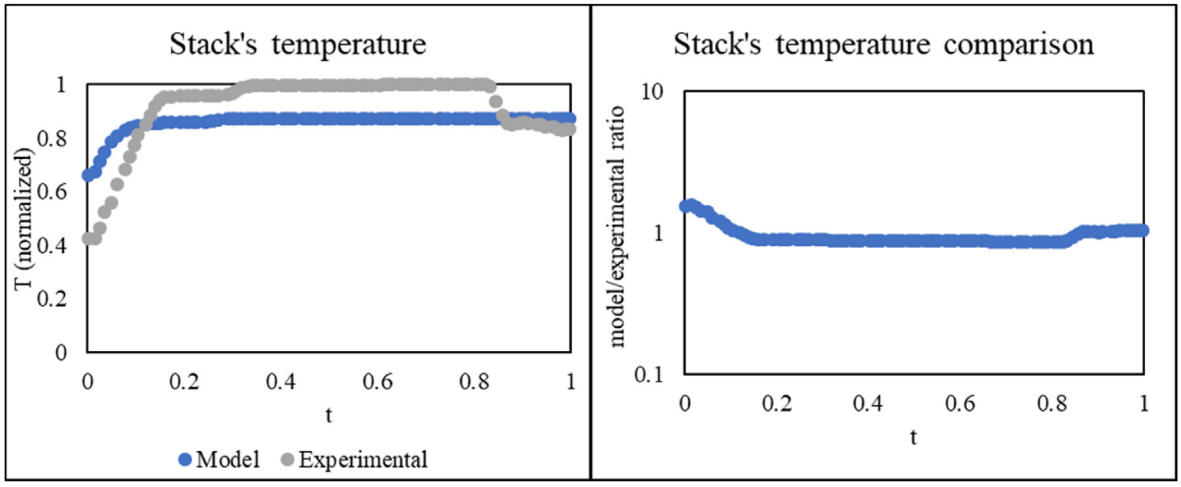

Fig. 11 – Normalized stack's temperature and model/experimental results ratio.

liquid-vapor equilibrium, being proportional to the separator's temperature. For this reason, it presents the same profile as the stack's temperature in Fig. 11.

To better represent thermal inertia, the ratio between each separator's temperature and the stack's is displayed in Fig. 15. H_2/electrolyte separator's temperature is slightly lower due to the intake of demineralized water in constant colder temperature.

best ratio of hydrogen produced by the stack's electricity cost. The price of electricity was determined for France in the year of 2019 as made available on the website www.entsoe.eu and it is shown in Fig. 16.

Objective function

As it is sought to maximize the ratio mentioned above, the objective function translates to:

$$\max \frac{\text{produced hydrogen gas in one year [mol]}}{\text{cost of electricity consumed by the stack in one year [kWh]}} = \max \frac{\int_0^{1\ \text{year}} V_{H2}^{s}\, dt}{\int_0^{1\ \text{year}} E\, dt} \tag{61}$$

Optimization

As a fictional scenario, it was determined that a minimum amount of hydrogen gas is to be produced in a year with the

The integration was implemented numerically through Gauss-Lobatto quadrature which is an approximation made possible through the same method employed for stablishing the

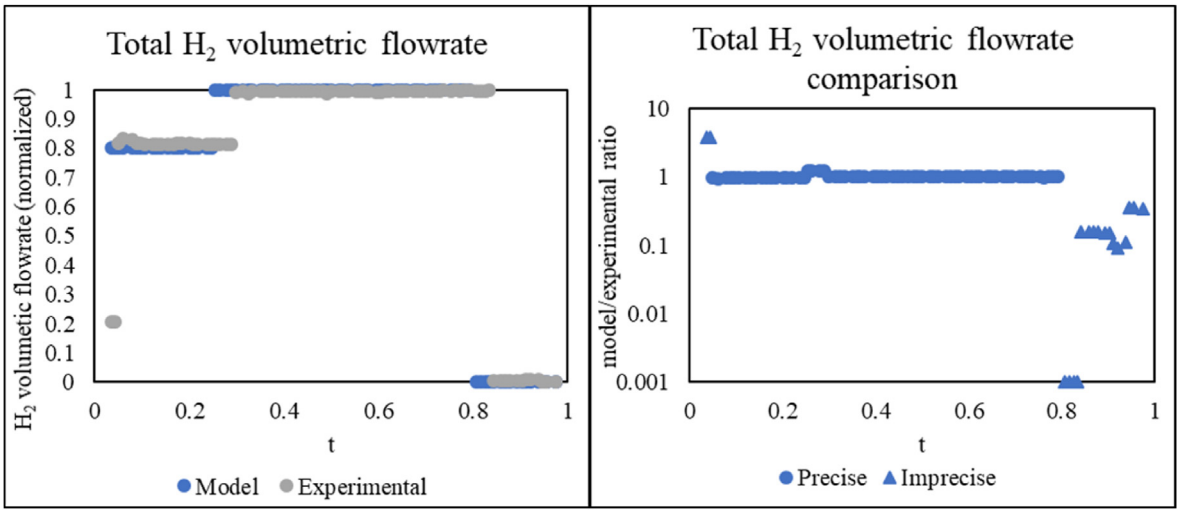

Fig. 12 – Normalized stack's total H_2 volumetric flow rate and model/experimental results ratio.

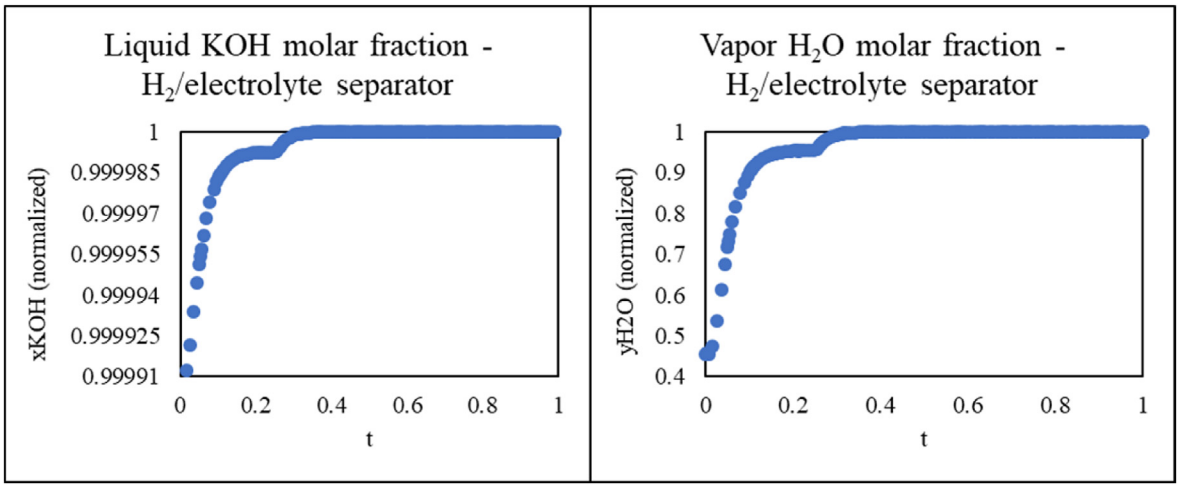

Fig. 13 – Normalized H_2/electrolyte liquid KOH and vapor H_2O molar fractions.

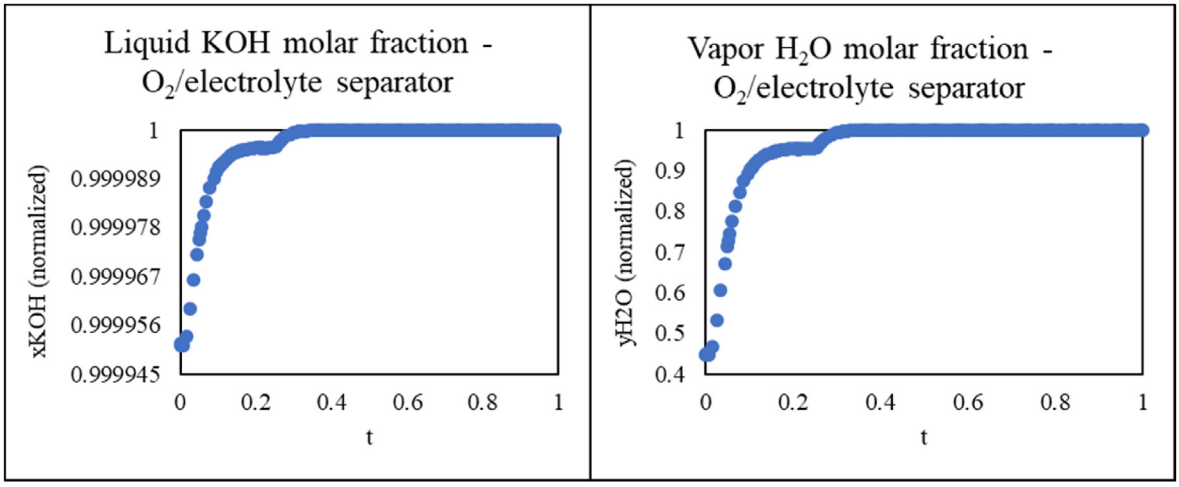

Fig. 14 – Normalized O_2/electrolyte liquid KOH and vapor H_2O molar fractions.

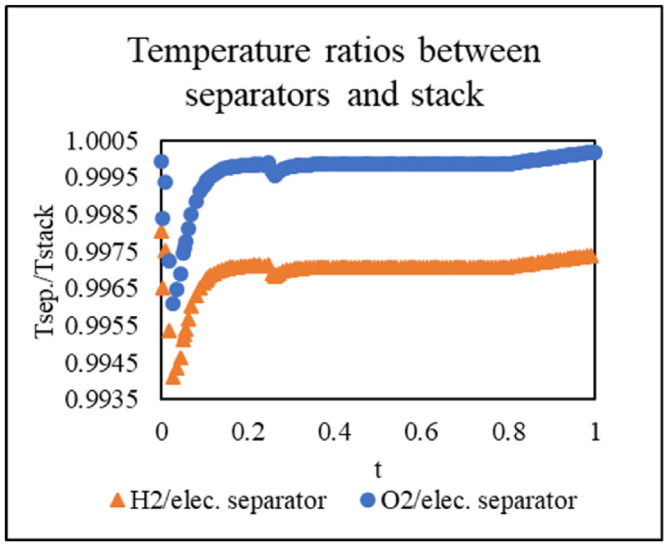

Fig. 15 – Temperature ratios between gas/electrolyte separators and the stack.

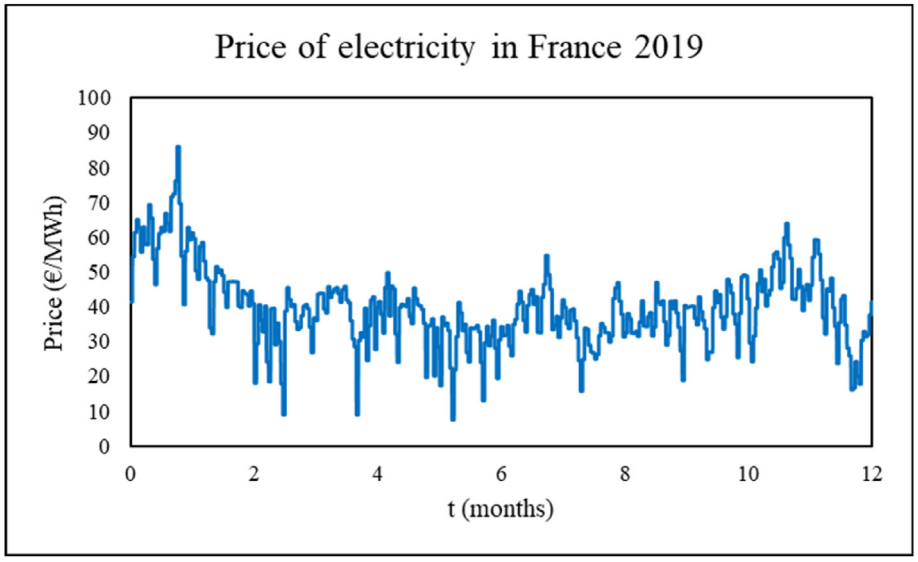

Fig. 16 – Price of electricity in France in 2019. Source: www.entsoe.eu.

positions of collocation points. The element's length L_f was set to 15 days.

Optimization variable

The excess variable with regard to the number of equations is the electrolysis unit's load. Whilst in simulation it was a parameter fixed by the user, now it is the variable whose solution is the answer to satisfying the objective function. This means that at the end of the optimization, a profile for the unit's load for one year will provide the best production/electricity cost ratio.

Additional constraints

As stated on the introduction for the paragraph 0, there must be a minimum quantity of total produced hydrogen gas in a year. This was translated as the constraint expressed in equation (17).

$$\int_0^{1\ \text{year}} \dot{V}^s_{H_2}\, dt \geq 20664 \cdot 10^3\ \text{mol} = 41328\ \text{kg} \tag{62}$$

Moreover, there are technical constraints associated to the equipment that prevent the electric current from being altered instantly. Mathematically, this translates to a cap to the current's derivative with respect to time, as is shown in equation (18).

$$\frac{dI}{dt} \leq 10^{-4}\ A \Big/ s \tag{63}$$

Optimization results

After a computing time of 11 min and 13 s in standard laptop computer setup, the optimized profile for the unit's load is

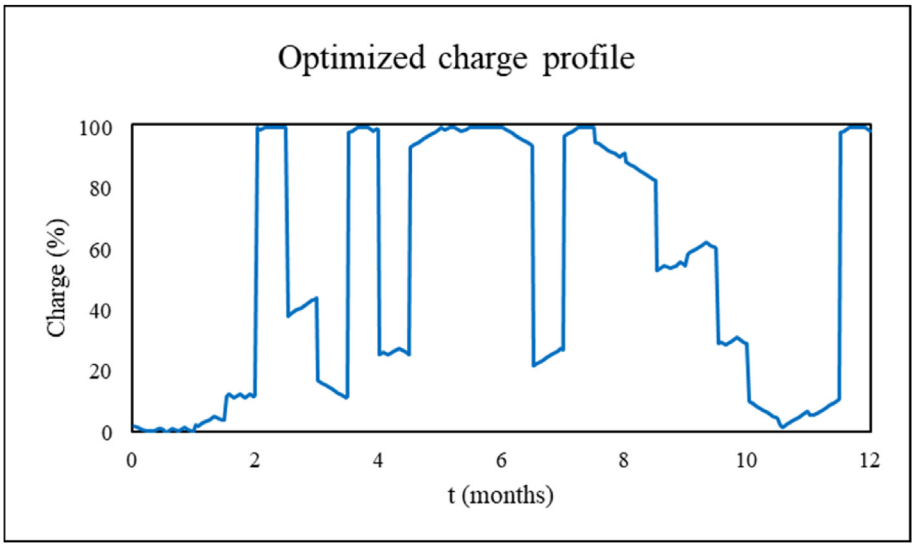

Fig. 17 – Profile of the electrolysis unit's optimal operating load profile.

represented in Fig. 17. As expected, maximum load was reached when electricity is cheaper and moderate loads were maintained when the price peaks. The optimized cost of electricity supplied to the stack is equal to € 70,455. This represents an economy of 17% in comparison to a scenario where the unit maintains a constant load to produce the same amount of hydrogen in one year.

Conclusion

A dynamic model was developed considering the accumulation of energy and matter in the three main processes of an alkaline electrolysis unit. The system composed of differential equations was converted into a set of nonlinear algebraic equations using the OCFE method. It was then validated by confrontation with real dynamic behavior. The modelling strategy developed for the methodology and modelling development is based on a standard electrolyzer configuration relying on numerous assumptions. However, in order to achieve a high level of representation, the model needs several technical specifications related to the equipment, which can be obtained in case of a strong partnership with electrolyzer manufacturers for instance. The optimization of the unit's load was executed aiming to reduce cost with electricity, showcasing the model's potential.

AMPL language and CONOPT solver were appropriate towards the problem's complexity since they found coherent solutions in an acceptable time span. These solutions indicate that energy accumulation has a much greater impact on the operation than mass holdup in the separators as electricity and utility consumptions are strictly connected to temperature.

The modelling approach has proven to be adaptable to the proposed dynamic optimization demands and is therefore a promising contribution the project's next goals, which involve the system's integration with other technologies.

Future work suggests improvements to the model such as adding thermal inertia due to piping and the separators' metal walls. Also, multiple simplifying assumptions may be revisited to address real operation issues like the mixing of O_2 and H_2 gas through electrolyte absorption. In addition, more realistic scenarios can be employed and different optimization variables could be created to explore the potential of this model towards the enhancement of an electrolysis unit operation. For instance, adding data related to renewables excess energy production throughout the year in a daily scale would render the scenario more accurate. This work's strategy is expected to be extended to other platforms comprising energy integration technologies.

Funding

This research did not receive any specific grant from funding agencies in the public, commercial, or not-for-profit sectors.

Declaration of competing interest

The authors declare that they have no known competing financial interests or personal relationships that could have appeared to influence the work reported in this paper.

Appendix A. Supplementary data

XXX

REFERENCES

[1] Ediger VŞ. An integrated review and analysis of multi-energy transition from fossil fuels to renewables. Energy Proc 2019;156:2–6. https://doi.org/10.1016/j.egypro.2018.11.073.

[2] Thiel GP, Stark AK. To decarbonize industry, we must decarbonize heat. Joule 2021;5:531–50. https://doi.org/10.1016/j.joule.2020.12.007.
[3] Xiao J, Li G, Xie L, Wang S, Yu L. Decarbonizing China's power sector by 2030 with consideration of technological progress and cross-regional power transmission. Energy Pol 2021;150:112150. https://doi.org/10.1016/j.enpol.2021.112150.
[4] Rodríguez-Sarasty JA, Debia S, Pineau P-O. Deep decarbonization in Northeastern North America: the value of electricity market integration and hydropower. Energy Pol 2021;152:112210. https://doi.org/10.1016/j.enpol.2021.112210.
[5] Gupta A, Davis M, Kumar A. An integrated assessment framework for the decarbonization of the electricity generation sector. Appl Energy 2021;288:116634. https://doi.org/10.1016/j.apenergy.2021.116634.
[6] Li D, Gao C, Chen T, Guo X, Han S. Planning strategies of power-to-gas based on cooperative game and symbiosis cooperation. Appl Energy 2021;288:116639. https://doi.org/10.1016/j.apenergy.2021.116639.
[7] Lazar MD, Mihet M, Dan M. Hydrogen to methane—an important step in the power-to-gas concept. In: Ref. Module Earth Syst. Environ. Sci. Elsevier; 2020. https://doi.org/10.1016/B978-0-12-819727-1.00032-7. B9780128197271001000.
[8] Xiong B, Predel J, Crespo del Granado P, Egging-Bratseth R. Spatial flexibility in redispatch: supporting low carbon energy systems with Power-to-Gas. Appl Energy 2021;283:116201. https://doi.org/10.1016/j.apenergy.2020.116201.
[9] Olivier P, Bourasseau C, PrB Bouamama. Low-temperature electrolysis system modelling: a review. Renew Sustain Energy Rev 2017;78:280–300. https://doi.org/10.1016/j.rser.2017.03.099.
[10] Lee J, Alam A, Ju H. Multidimensional and transient modeling of an alkaline water electrolysis cell. Int J Hydrogen Energy 2021;46:13678–90. https://doi.org/10.1016/j.ijhydene.2020.10.133.
[11] Zarghami A, Deen NG, Vreman AW. CFD modeling of multiphase flow in an alkaline water electrolyzer. Chem Eng Sci 2020;227:115926. https://doi.org/10.1016/j.ces.2020.115926.
[12] Górecki K, Górecki P, Zarębski J. Electrical model of the alkaline electrolyser dedicated for SPICE. Int J Circ Theor Appl 2018;46:1044–54. https://doi.org/10.1002/cta.2459.
[13] Ursúa A, Sanchis P. Static–dynamic modelling of the electrical behaviour of a commercial advanced alkaline water electrolyser. Int J Hydrogen Energy 2012;37:18598–614. https://doi.org/10.1016/j.ijhydene.2012.09.125.
[14] Amores E, Rodríguez J, Oviedo J, de Lucas-Consuegra A. Development of an operation strategy for hydrogen production using solar PV energy based on fluid dynamic aspects. Open Eng 2017;7:141–52. https://doi.org/10.1515/eng-2017-0020.
[15] Jang D, Choi W, Cho H-S, Cho WC, Kim CH, Kang S. Numerical modeling and analysis of the temperature effect on the performance of an alkaline water electrolysis system. J Power Sources 2021;506:230106. https://doi.org/10.1016/j.jpowsour.2021.230106.
[16] Jang D, Cho H-S, Kang S. Numerical modeling and analysis of the effect of pressure on the performance of an alkaline water electrolysis system. Appl Energy 2021;287:116554. https://doi.org/10.1016/j.apenergy.2021.116554.
[17] Varela C, Mostafa M, Zondervan E. Modeling alkaline water electrolysis for power-to-x applications: a scheduling approach. Int J Hydrogen Energy 2021;46:9303–13. https://doi.org/10.1016/j.ijhydene.2020.12.111.
[18] Järvinen L, Puranen P, Kosonen A, Ruuskanen V, Ahola J, Kauranen P, et al. Automized parametrization of PEM and alkaline water electrolyzer polarisation curves. Int J Hydrogen Energy 2022;47:31985–2003. https://doi.org/10.1016/j.ijhydene.2022.07.085.
[19] Amores E, Rodríguez J, Carreras C. Influence of operation parameters in the modeling of alkaline water electrolyzers for hydrogen production. Int J Hydrogen Energy 2014;39:13063–78. https://doi.org/10.1016/j.ijhydene.2014.07.001.
[20] David M, Alvarez H, Ocampo-Martinez C, Sánchez-Peña R. Dynamic modelling of alkaline self-pressurized electrolyzers: a phenomenological-based semiphysical approach. Int J Hydrogen Energy 2020;45:22394–407. https://doi.org/10.1016/j.ijhydene.2020.06.038.
[21] Haug P, Kreitz B, Koj M, Turek T. Process modelling of an alkaline water electrolyzer. Int J Hydrogen Energy 2017;42:15689–707. https://doi.org/10.1016/j.ijhydene.2017.05.031.
[22] Sakas G, Ibáñez-Rioja A, Ruuskanen V, Kosonen A, Ahola J, Bergmann O. Dynamic energy and mass balance model for an industrial alkaline water electrolyzer plant process. Int J Hydrogen Energy 2022;47:4328–45. https://doi.org/10.1016/j.ijhydene.2021.11.126.
[23] Henao C, Agbossou K, Hammoudi M, Dubé Y, Cardenas A. Simulation tool based on a physics model and an electrical analogy for an alkaline electrolyser. J Power Sources 2014;250:58–67. https://doi.org/10.1016/j.jpowsour.2013.10.086.
[24] Abdin Z, Webb CJ, Gray EMacA. Modelling and simulation of an alkaline electrolyser cell. Energy 2017;138:316–31. https://doi.org/10.1016/j.energy.2017.07.053.
[25] Ren Z, Wang J, Yu Z, Zhang C, Gao S, Wang P. Experimental studies and modeling of a 250-kW alkaline water electrolyzer for hydrogen production. J Power Sources 2022;544:231886. https://doi.org/10.1016/j.jpowsour.2022.231886.
[26] Phillips R, Edwards A, Rome B, Jones DR, Dunnill CW. Minimising the ohmic resistance of an alkaline electrolysis cell through effective cell design. Int J Hydrogen Energy 2017;42:23986–94. https://doi.org/10.1016/j.ijhydene.2017.07.184.
[27] Mansilla C, Dautremont S, Shoai Tehrani B, Cotin G, Avril S, Burkhalter E. Reducing the hydrogen production cost by operating alkaline electrolysis as a discontinuous process in the French market context. Int J Hydrogen Energy 2011;36:6407–13. https://doi.org/10.1016/j.ijhydene.2011.03.004.
[28] de Groot MT, Kraakman J, Garcia Barros RL. Optimal operating parameters for advanced alkaline water electrolysis. Int J Hydrogen Energy 2022;47:34773–83. https://doi.org/10.1016/j.ijhydene.2022.08.075.
[29] Coutanceau C, Baranton S, Audichon T. Hydrogen production from water electrolysis. Hydrog. Electrochem. Prod.. Elsevier; 2018. p. 17–62. https://doi.org/10.1016/B978-0-12-811250-2.00003-0.
[30] Amores E. 9. Renewable hydrogen production by water electrolysis n.d.:43.
[31] Sánchez M, Amores E, Abad D, Rodríguez L, Clemente-Jul C. Aspen Plus model of an alkaline electrolysis system for hydrogen production. Int J Hydrogen Energy 2020;45:3916–29. https://doi.org/10.1016/j.ijhydene.2019.12.027.
[32] Santos DMF, Sequeira CAC, Figueiredo JL. Hydrogen production by alkaline water electrolysis. Quím Nova 2013;36:1176–93. https://doi.org/10.1590/S0100-40422013000800017.
[33] Barco-Burgos J, Eicker U, Saldaña-Robles N, Saldaña-Robles AL, Alcántar-Camarena V. Thermal characterization of an alkaline electrolysis cell for hydrogen production at

atmospheric pressure. Fuel 2020;276:117910. https://doi.org/10.1016/j.fuel.2020.117910.
[34] Jang D, Choi W, Cho H-S, Cho WC, Kim CH, Kang S. Numerical modeling and analysis of the temperature effect on the performance of an alkaline water electrolysis system. J Power Sources 2021;506:230106. https://doi.org/10.1016/j.jpowsour.2021.230106.
[35] Brauns J, Turek T. Alkaline water electrolysis powered by renewable energy: a review. Processes 2020;8:248. https://doi.org/10.3390/pr8020248.
[36] Milewski J, Guandalini G, Campanari S. Modeling an alkaline electrolysis cell through reduced-order and loss-estimate approaches. J Power Sources 2014;269:203–11. https://doi.org/10.1016/j.jpowsour.2014.06.138.
[37] Davis RE. The solubility and diffusion coefficient of oxygen in potassium hydroxide solutions. 1967. p. 11.
[38] Ruetschi P, Amlie RF. Solubility of hydrogen in potassium hydroxide and sulfuric acid. Salting-Out and hydration. J Phys Chem 1966;70:718–23. https://doi.org/10.1021/j100875a018.
[39] Balej J. Water vapour partial pressures and water activities in potassium and sodium hydroxide solutions over wide concentration and temperature ranges. 1985. p. 11.
[40] Hnedkovsky L, Bochmann S, May PM, Hefter G. Molar volumes and heat capacities of aqueous solutions of potassium hydroxide and for water ionization up to 573 K at 10 MPa. J Chem Eng Data 2017;62:2959–72. https://doi.org/10.1021/acs.jced.7b00192.
[41] Akerlof G, Bender P. The density of aqueous solutions of potassium hydroxide. J Am Chem Soc 1941;63:1085–8. https://doi.org/10.1021/ja01849a054.
[42] Todd B, Young JB. Thermodynamic and transport properties of gases for use in solid oxide fuel cell modelling. J Power Sources 2002;110:186–200. https://doi.org/10.1016/S0378-7753(02)00277-X.

Nomenclature

Latin characters

B1: molar flowrate of the stack's biphasic stream leading to the oxygen/electrolyte separator (mol s^{-1})
B2: molar flowrate of the stack's biphasic stream leading to the hydrogen/electrolyte separator (mol s^{-1})
Cp_i^L: liquid specific heat of constituent i (J mol^{-1} K^{-1})
Cp_i^V: vapor specific heat of constituent i (J mol^{-1} K^{-1})
d_1: parameter related to ohmic resistance (Ω m^2)
d_2: parameter related to ohmic resistance (Ω m^2 bar^{-1})
E: power supplied to the stack (W)
F: Faraday constant (C mol^{-1})
h_{St}^e: stack's electrolyte inlet specific enthalpy (J mol^{-1})
h^L: liquid specific enthalpy (J mol^{-1})
h^M: steel's specific enthalpy (J kg^{-1})
H^{B1}: biphasic stream B1's specific enthalpy (J mol^{-1})
H^{B2}: biphasic stream B2's specific enthalpy (J mol^{-1})
H^V: separators' vapor phase specific enthalpy (J mol^{-1})
H^{V1}: stack's oxygen vapor phase specific enthalpy (J mol^{-1})
H^{V2}: stack's hydrogen vapor phase specific enthalpy (J mol^{-1})
i: electric current density (A m^{-2})
I: electric current (A)
K_ξ: reaction's extent constant (A s mol^{-1})
Kv: valve's constant (m3 s^{-1} $Pa^{-1/2}$)
L_{St}^e: molar flowrate of the stack's electrolyte inlet (mol s^{-1})
$L_{SeH2}^{e,H2O}$: molar flowrate of demineralized water inlet (mol s^{-1})
L_f: finite element's length (s)
L_{SeH2}^s: molar flowrate of hydrogen/electrolyte's liquid outlet (mol s^{-1})
ℓ_j: Lagrange's polynomial for the collocation point j
M: mass of the stack's steel structure (kg)
m^L: liquid phase's mass holdup (kg)
$Mmol_i$: molar mass of constituent i (g/mol)
M_x: collocation matrix
n_f: number of finite elements
n_j: last collocation point's position
N^L: molar holdup of the liquid phase (mol)
N^V: molar holdup of the vapor phase (mol)
Ov: valve's opening
P: equipment pressure (Pa)
P_i^{sat}: saturation pressure for constituent i (Pa)
p: pressure for the cell's voltage model (bar)
R: universal gas constant (J mol^{-1} K^{-1})
r_1: parameter related to ohmic resistance (Ω m^2)
r_2: parameter related to ohmic resistance (Ω m2 K^{-1})
s: coefficient for overvoltage on electrodes (V)
t: time (s)
T: equipment temperature (K)
T_{eb}: boiling temperature (K)
T^{Le}: demineralized water inlet's temperature (K)
T_{ref}: reference temperature (K)
t_1: coefficient for overvoltage on electrodes (m^2 A^{-1})
t_2: coefficient for overvoltage on electrodes (m^2 K A^{-1})
t_3: coefficient for overvoltage on electrodes (m^2 K^2 A^{-1})
U_{rev}: reversible voltage (V)
U_{cell}: electrolytic cell's voltage (V)
$\dot{V}_{gas}$: volumetric flowrate passing through separators' valves (m^3 s^{-1})
V^{liq}: separator's liquid volume (m^3)
V_{H2}^s: molar flowrate of hydrogen's heat exchanger vapor outlet (mol s^{-1})
V_{SeH2}^s: molar flowrate of hydrogen/electrolyte separator's vapor outlet (mol s^{-1})
V_{SeO2}^s: molar flowrate of oxygen/electrolyte separator's vapor outlet (mol s^{-1})
V^{tot}: total separator's volume (m^3)
V^{vap}: separator's vapor volume (m^3)
x_i: liquid molar fraction of constituent i
x_i^{B1}: liquid molar fraction of constituent i in the liquid phase of the biphasic stream B1
x_i^{B2}: liquid molar fraction of constituent i in the liquid phase of the biphasic stream B2
$x_i^{Le,H2O}$: liquid molar fraction of constituent i in demineralized water inlet
y_i: vapor molar fraction of constituent i
y_i^{B1}: vapor molar fraction of constituent i in the vapor phase of the biphasic stream B1
y_i^{B2}: vapor molar fraction of constituent i in the vapor phase of the biphasic stream B2
z: moles of electrons transferred for the production of 1 mol of H_2
z_i^{B1}: molar fraction of constituent i in biphasic stream B1
z_i^{B2}: molar fraction of constituent i in biphasic stream B2

Greek characters

ΔG: water electrolysis Gibbs free energy (kJ mol^{-1})
Δg^0: water electrolysis standard Gibbs free energy (kJ mol^{-1})
ΔH^{reac}: water electrolysis enthalpy of reaction (kJ mol^{-1})
Δh^0: water electrolysis standard enthalpy of reaction (kJ mol^{-1})
ΔP: pressure difference between the two sides of a valve (Pa)
ΔS: water electrolysis entropy (kJ mol^{-1} K^{-1})
Δs^0: water electrolysis standard entropy (kJ mol^{-1} K^{-1})
ν_i: stoichiometric coefficient of constituent i on electrolysis global reaction
ξ: normalized integration variable
ω^{B1}: vapor fraction of stream B1
ω^{B2}: vapor fraction of stream B2